Applied Catalysis B: Environmental 191 (2016) 8–17

Contents lists available at ScienceDirect

Applied Catalysis B: Environmental

journal homepage: www.elsevier.com/locate/apcatb

CO_2 hydrogenation to methanol over $Cu/ZnO/ZrO_2$ catalysts prepared by precipitation-reduction method

Xiaosu Dong[a,b], Feng Li[a,*], Ning Zhao[a,c,*], Fukui Xiao[a,c], Junwei Wang[a,c], Yisheng Tan[a,c]

[a] State Key Laboratory of Coal Conversion, Institute of Coal Chemistry, Chinese Academy of Sciences, South Taoyuan Road 27#, Taiyuan 030001, PR China
[b] University of Chinese Academy of Sciences, Beijing 100049, PR China
[c] National Engineering Research Center for Coal-based Synthesis, Taiyuan 030001, PR China

ARTICLE INFO

Article history:
Received 12 November 2015
Received in revised form 6 March 2016
Accepted 7 March 2016
Available online 9 March 2016

Keywords:
Precipitation-reduction method
$NaBH_4$
$Cu/ZnO/ZrO_2$ catalysts
CO_2 hydrogenation
Methanol

ABSTRACT

A series of $Cu/ZnO/ZrO_2$ catalysts were prepared by precipitation-reduction method and tested for the synthesis of methanol by CO_2 hydrogenation. The advantages of precipitation-reduction method over conventional co-precipitation method, the effect of $NaBH_4$ content were investigated by XRD, N_2 physisorption, SEM, TEM, N_2O chemisorption, XPS, TPR, CO_2-TPD techniques. The influence of precipitation-reduction process on the average Cu particle size, aggregation state and interaction among different elements were discussed in detail. The content of $NaBH_4$ had an effect on the exposed Cu surface area as well as the ratio of Cu^0/Cu^+ and thus influenced the catalytic performance. The catalysts prepared by precipitation-reduction method increased the number of basic sites and had a significant advantage in methanol selectivity in contrast with conventional precipitation method. A suitable $NaBH_4$ content was beneficial to the catalytic performance in $Cu/ZnO/ZrO_2$ catalysts and a maximum space time yield of CH_3OH was obtained with B/Cu = 5 at 543 K.

1. Introduction

Global warming caused by the increase of atmospheric CO_2 concentration and the depletion of fossil fuel are becoming great challenges to the development of modern society. Catalytic conversion of CO_2 to methanol is a promising route that may offer a solution to the green-house gas mitigation and fossil fuel substitution [1,2]. The optimization of catalysts has been a key research to improve the catalytic performance.

Conventional $Cu/ZnO/Al_2O_3$ catalysts prepared by co-precipitation method are employed predominantly in the industrial low-temperature methanol synthesis process [3,4]. As a promising support and promoter, zirconia has a weak hydrophilic character in comparison to alumina, which could enhance the copper dispersion as well as the surface basicity [5–9]. As a result, $Cu/ZnO/ZrO_2$ catalysts are particularly effective in the hydrogenation of CO_2 to methanol. The catalyst composition [7,10–13], preparation method [3,14–17] and pretreatment [18,19] have considerable influences on the catalytic performance. Although the reduction procedure is important, little research is reported. General methods for the preparation of metallic catalyst are to reduce metal oxide with H_2 or CO at high temperature. Unfortunately, the conventional gas phase reduction process of copper-based catalysts has the characteristics of intense heating effect, time-consuming operation and unmanageable reducing conditions, which could accelerate the agglomeration of surface active sites or the fast growth of particles, especially at high temperature [20]. Then, other reduction processes have been explored to improve the catalytic performance. Fujita et al. reported that using methanol as the reducing agent was better than using H_2 in CO_2 hydrogenation to methanol [18]. Shi et al. obtained Cu/ZnO catalysts by a novel solid-state combustion method and the results showed that the components were converted to metallic Cu^0 and ZnO species without further reduction over which the catalytic activity and methanol selectivity for low temperature methanol synthesis from syngas containing CO_2 were significantly improved compared with conventional solid-state reduction method [21–23]. Recently, an attractive technique to reduce the copper-based catalysts with $NaBH_4$ has been proposed, which is economic, rapid and easy to operate in comparison to gas phase reduction. Belin et al. found that $CuAu/SiO_2$ catalysts reduced by $NaBH_4$ led to small particles and thus exhibited higher activity for the selective oxidation of propene to acrolein compared with reduction by H_2 [24]. Moreover, as reported by Liaw and coworkers, ultrafine Cu-based catalysts prepared by chemical reduction with $NaBH_4$ were employed in methanol synthesis from CO_2/H_2 using a slurry reactor in the liquid phase [25].

* Corresponding authors.
E-mail addresses: lifeng2729@sxicc.ac.cn (F. Li), zhaoning@sxicc.ac.cn (N. Zhao).

http://dx.doi.org/10.1016/j.apcatb.2016.03.014
0926-3373/

The active sites over the Cu-based catalysts for CO_2 hydrogenation to methanol are considered to be Cu^0, Cu^+ or Cu^0 and Cu^+. Many researchers have pointed that metallic Cu is the active site and the activity is found to be directly proportional to the Cu surface area [26–28]. However, many researchers reported that the catalytic activity was relevant to the Cu surface area but not in a linear relationship. Herman et al. found that active Cu^+ sites were dissolved on the surface of ZnO matrix,which thereby stabilized Cu^+ and improved the catalytic performance [29]. Although there is not a consensus on this controversy, the point of both Cu^+ and Cu^0 species being believed to contribute to the activity of Cu-based catalysts is generally accepted [30–34]. Therefore, a proper ratio of Cu^0 and Cu^+ is important for the catalytic performance in CO_2 hydrogenation to methanol. Toyir et al. prepared gallium-promoted copper-based catalysts by impregnation method and found that the ratio of Cu^0/Cu^+ could be regulated by varying Ga content thus improved the catalytic performance in CO_2 hydrogenation to methanol [32,33]. So, the quantity of reducing agent is worthy to be explored and the reduction degree can be adjusted by varying $NaBH_4$ content during the precipitation-reduction process, thus the ratio of Cu^0/Cu^+ for the catalysts could be optimized to a certain extent.

In this paper, a series of $Cu/ZnO/ZrO_2$ catalysts reduced by $NaBH_4$ with different content were prepared and tested for the synthesis of methanol from CO_2/H_2. The catalysts were characterized by XRD, N_2 physisorption, SEM, TEM, N_2O chemisorption, XPS, TPR, CO_2-TPD techniques. A systematic investigation of the advantages of precipitation-reduction method over conventional co-precipitation method, the effect of $NaBH_4$ content on the structure and physicochemical properties is conducted to shed light into the structure-activity relationship of CO_2 hydrogenation to methanol in $Cu/ZnO/ZrO_2$ system.

2. Experimental

2.1. Preparation of catalysts

The $Cu/ZnO/ZrO_2$ catalysts with the mole ratio of $Cu^{2+}:Zn^{2+}:Zr^{4+} = 6:3:1$ were synthesized by co-precipitation method. Typically, a solution of Cu(II), Zn(II) and Zr(IV) nitrates (1 M, 80 mL) and a solution of Na_2CO_3 precipitant (1.2 M) were added dropwise to deionized water (80 mL) simultaneously under stirring at 338 K. The pH during precipitation was kept at a constant value of 7.0 ± 0.2. Reducing agent solution was prepared by a certain content $NaBH_4$ dissolved in 100 mL 0.1 M NaOH solution for the inhibition of hydrolysis. After the air in above system was evacuated, reducing agent solution was added dropwise to the precipitate under the protection of N_2 at 338 K. The color of the precipitate slurry transformed to black from bluish-green during precipitation-reduction process. The resulted slurry was then aged at 338 K for 2 h followed by filtering and washing with deionized water for five times till no Na^+ was detected. Finally, the filter cakes were dried for 10 h at 323 K in vacuum oven and then calcined at 573 K for 6 h under N_2 flow. The as-synthesized catalysts were denoted as CZZ-x (x is the $NaBH_4$/Cu molar ratio).

2.2. Characterization methods

Powder X-ray diffraction (XRD) were analyzed in the 2θ range 5°–75° using a Panalytical X'Pert Pro X-ray diffractometer with Cu Kα radiation, operating at 40 kV and 30 mA and in the step mode (0.0167°, 12 s).

Thermal gravimetric analysis (TG) were measured with a SETSYS EVOLUTION TGA 16/18 thermal analyzer. The samples were heated from room temperature to 1000 K at a heating rate of 10 K/min under Ar atmosphere.

The specific surface area (SA) and pore volume (PV) were determined from N_2 adsorption-desorption isotherms at 77 K, using a Micromeritics Tristar 3000 instrument. Samples degassing was carried out at 473 K prior to acquisition of the adsorption isotherm. The isotherms were elaborated by the BET method for surface area calculation, and BJH method was used to obtain pore size.

The morphology of the catalysts was investigated with a FET XL 30S-FEG scanning electron microscopy (SEM) with an accelerating voltage of 10.0 kV.

TEM, dark-field scanning TEM (STEM) and energy dispersive X-ray spectroscopy (EDS) measurements were carried out on a JEM-2100F high resolution transmission electron microscopy operated at 200.0 kV.

X-ray photoelectron spectroscopy (XPS) was performed on an AXIS ULTRA DLD spectrometer with a monochromatic Al Kα (1486.8 eV) source. The obtained binding energies were calibrated using the C1s peak (284.6 eV) as the reference. The experimental error is within ±0.1 eV.

Temperature programmed reduction (TPR) was performed in a quartz reactor with a thermal conductivity detector to record the consumption of H_2. The samples (50 mg) were reduced in a flow

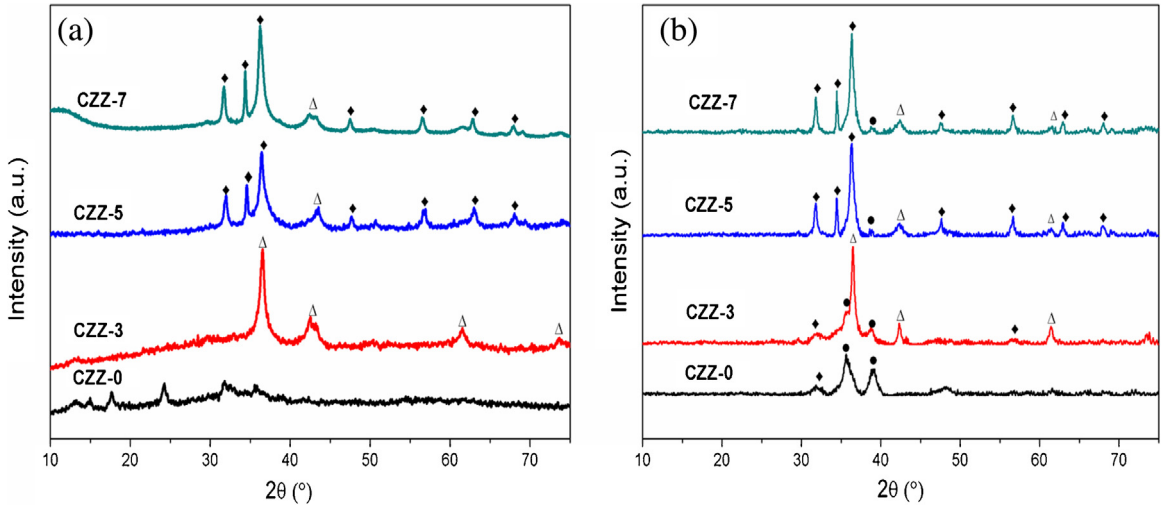

Fig. 1. XRD patterns of (a) dried and (b) calcined $Cu/ZnO/ZrO_2$ catalysts. (●) CuO; (△) Cu_2O; (♦) ZnO.

of 10 vol.% H_2/Ar at a heating rate of 5 K min^{-1} up to 723 K after pretreatment with Ar at 423 K for 1 h.

CO_2 temperature programmed desorption (CO_2-TPD) measurements were carried out on an AMETEK mass spectrometer to monitor the desorption of CO_2. All the samples were reduced at 503 K for 2 h with feed gas (H_2:CO_2 = 3:1). After cooling to room temperature, the catalysts were saturated in CO_2 flow at 323 K for 1 h and then flushed with Ar to remove the physical adsorbed molecules. The desorption processes were performed with a heating rate of 10 K min^{-1} under Ar flow up to 573 K and were recorded by the mass spectrometer.

The exposed Cu surface area (S_{Cu}) was determined by dissociative N_2O adsorption and carried out in a U-tube quartz reactor with a thermal conductivity detector (TCD) to monitor the consumption of H_2. The catalysts (100 mg) were first reduced in 10 vol.% H_2/Ar mixture for 2 h at 503 K and then cooled to room temperature with Ar flow. The samples were exposed to N_2O for 1 h at 323 K to ensure complete oxidation of metallic copper to Cu^+ and then cooled down to room temperature with Ar flow. Finally, the catalysts were reduced again in 10 vol.% H_2/Ar mixture with a temperature programmed reduction to 573 K (5 K/min) and the amount of consumed H_2 was denoted as n_{H_2}. The exposed Cu surface area (S_{Cu}) was calculated by the equations

$$n_{Cu} = 2n_{H_2}$$

$$S_{Cu} = (n_{Cu} \times N)/(1.4 \times 10^{19} \times W)(m^2\,g^{-1})$$

where S_{Cu} is the exposed copper surface area per gram catalyst, n_{Cu} is the amount of surface metallic copper of the catalyst, N is Avogadro's constant (6.02×10^{23} atoms mol^{-1}), 1.4×10^{19} is the number of copper atoms per square meter, and W is the quantity of catalyst [35].

2.3. Catalytic evaluation of catalysts

The activity evaluation of the catalysts for CO_2 hydrogenation to methanol were carried out in a continuous-flow, high pressure, fixed-bed reactor. Catalyst (1.0 mL, 40–60 mesh) diluted with equal volume quartz sand was placed in a stainless steel tube reactor. The activities of catalysts in CO_2 hydrogenation to methanol reaction were determined under 503–543 K, 5.0 MPa, $n(H_2)$: $n(CO_2)$ = 3:1, and GHSV = 4600 h^{-1}. Before activity test, CZZ-0 sample was reduced in pure H_2 under atmospheric pressure at 503 K for 4 h, while CZZ-3, CZZ-5 and CZZ-7 samples were directly tested without further H_2-reduction process. After a reaction of 24 h on stream, products were quantitatively analyzed with gas chromatograph with a thermal conductivity detector. Gas products of H_2, CO_2, CO and CH_4 were detected by TDX-01 column and liquid products of H_2O and CH_3OH were detected by Porapak-Q column. The CO_2 conversion and the carbon-based selectivity of CH_3OH and CO were calculated by an internal normalization method. The space time yield (STY) of CH_3OH, which gave the amount of CH_3OH produced per milliliter catalyst per hour, was defined as

$$STY_{CH_3OH} = (W \times X_{CH_3OH})/(t \times V)\left(gmL^{-1}h^{-1}\right)$$

where W is the total weight of H_2O and CH_3OH (g); X_{CH_3OH} is the mass fraction of CH_3OH; t is the reaction time (h); V is the volume of catalyst (mL).

3. Results and discussions

3.1. Textural and structural properties

The XRD patterns of dried and calcined Cu/ZnO/ZrO_2 catalysts are shown in Fig. 1(a) and (b), respectively. As shown in Fig. 1(a), the precursor structure of CZZ-0 sample obtained from conventional co-precipitation method is zincian-malachite [$(Cu,Zn)_2(OH)_2CO_3$] (JCPDS # 17-0216). However, for dried samples prepared by precipitation-reduction method, diffraction peaks ascribed to Cu_2O phase (JCPDS # 05-0667) and a crystallized ZnO phase (JCPDS # 36-1451) are observed in CZZ-3 ~ 7 samples, illustrating that Cu^{2+} in the co-precipitation system is partially reduced. Furthermore, the hydroxyl carbonate precursors turn into metal oxides during the liquid reduction process. Actually, the Cu/ZnO/ZrO_2 catalysts prepared by co-precipitation are usually mixed metal oxides after calcination despite of the phase of the precursors [36,37]. In this study, some broad diffraction peaks at 2θ = 35.5°, 39.0° attributed to a crystallized CuO phase (JCPDS # 45-0937) and a poorly crystallized ZnO phase are detected in CZZ-0 sample after calcination while ZrO_2 exists as an amorphous state, as shown in Fig. 1(b), which is consistent with other reports [8,12]. With increasing $NaBH_4$ amount, more hydrogen is produced in the reduction process, contributing to the dispersion of Cu_2O. Therefore, the intensity of diffraction peaks assigned to Cu_2O phase decreases from B/Cu = 3 to 7 in Fig. 1(b). Interestingly, the intensity of diffraction peaks attributed to ZnO phase increases dramatically when B/Cu ≥ 5, suggesting that the amorphous ZnO phase has grown into a crystal form, thus the interaction between copper and zinc is changed.

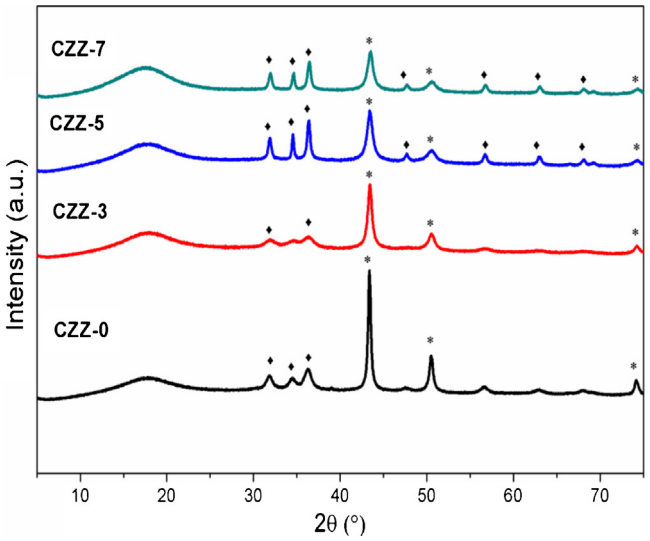

Fig. 2. XRD patterns of the Cu/ZnO/ZrO_2 catalysts after treatment with gas phase. (*) Cu; (♦) ZnO.

The XRD patterns of CZZ-0 sample reduced in H_2 at 503 K for 2 h and CZZ-3 ~ 7 samples treated in feed gas (H_2:CO_2 = 3:1) at 503 K for 2 h are shown in Fig. 2. The typical diffraction peaks at 2θ = 43.3°, 50.4° and 74.1°, are attributed to (1 1 1), (2 0 0) and (2 2 0) crystal planes of a crystallized Cu phase (JCPDS # 04-0836). A well crystallized Cu phase and a poorly crystallized ZnO phase are detected in CZZ-0 sample, manifesting that the treatment with H_2 leads to the reduction of CuO to Cu. After treatment with feed gas, the typical diffraction peaks assigned to CuO and Cu_2O disappear and a crystallized Cu phase emerges in CZZ-3 ~ 7 samples, implying that the precipitation-reduction process has not reduced Cu species thoroughly and the treatment with feed gas results in a secondary gas phase reduction. Furthermore, the intensity of diffraction peaks attributed to Cu phase continuously decreases with B/Cu from 0 to 7. It can be concluded that the growth of metallic Cu grain crystals of catalysts which are reduced by $NaBH_4$ beforehand can be restrained to some extent when undergoing gas phase treatment at high temperature and this inhibiting effect strengthens with increasing $NaBH_4$ content. In other words, the

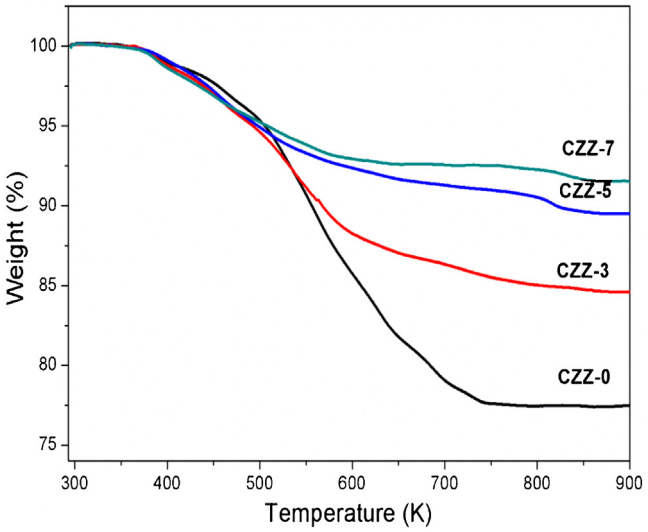

Fig. 3. Thermogravimetry profiles of dried $Cu/ZnO/ZrO_2$ catalysts.

precipitation-reduction process plays a buffer role on the growth of Cu grain crystals against thermal treatment with gas phase.

TG analysis was performed to investigate the decomposition behavior of the dried precursors. The TG pattern is shown in Fig. 3 and the total weight loss (%) is listed in Table 1. The tendency of weight loss pattern between CZZ-0 sample and CZZ-3 ~ 7 samples is similar while the quantity of weight loss is obvious different. The weight loss in the range from 300 K to 500 K is derived from the loss of water. The CZZ-0 sample, prepared by conventional co-precipitation method, exhibits the maximum weight loss (ca. 22.8 wt%) which mainly attributed to the decomposition of the zincian-malachite phase. With increasing B/Cu from 3 to 7, the total weight loss presents a decrease from 15.7% to 8.9%. As shown in XRD results, most hydroxyl carbonate precursors are transformed to metal oxides during the liquid reduction procedure. In addition, this transformation effect of liquid reduction procedure strengthens with the elevation of $NaBH_4$ content, as evidenced by the decrease of weight loss for CZZ-3 ~ 7 samples. So, the weight loss of samples obtained from precipitation-reduction method is attributed to the loss of water and the decomposition of hydroxyl carbonate residues.

The physicochemical properties of the $Cu/ZnO/ZrO_2$ catalysts are listed in Table 1. The specific surface area of the catalysts decreases with increasing $NaBH_4$ content. It can be seen that the metal copper surface area (S_{Cu}) calculated by N_2O dissociative adsorption of CZZ-0 sample is higher than that of other samples. While for CZZ-3 ~ 7 samples, S_{Cu} increases first and then decreases with the elevation of $NaBH_4$ content. The average Cu grain crystals size calculated by Cu (111) reflection in the XRD results using Scherrer equation exhibits a declining tendency with the increase of $NaBH_4$ content.

Fig. 4 shows the SEM images of the $Cu/ZnO/ZrO_2$ catalysts. Aggregated spherical particles are observed in CZZ-0 sample, while well dispersed particles are found for CZZ-3 ~ 7 samples. On further $NaBH_4$ content increase, ongoing growth of particles is seen, which is in good agreement with the N_2 physisorption results. Furthermore, rodlike particles begin to appear when $B/Cu \geq 5$.

TEM images of the catalysts are shown in Fig. 5. It can be seen that the CZZ-0 sample exhibits uniform particle size distribution in the range of 8–11 nm, while the spherical particles grow to 30–50 nm for CZZ-3 ~ 7 samples. The particle size grows with increasing $NaBH_4$ content, which is in accordance with the SEM results. The rodlike particles emerged in CZZ-5 and CZZ-7 reach a length of 200–300 nm, and their dimension as well as quantity increase with increasing $NaBH_4$ content.

Fig. 6(a) shows the STEM image of CZZ-5 sample where some spherical particles are around rodlike particle. It can be observed that Cu mainly concentrates in spherical particles while the

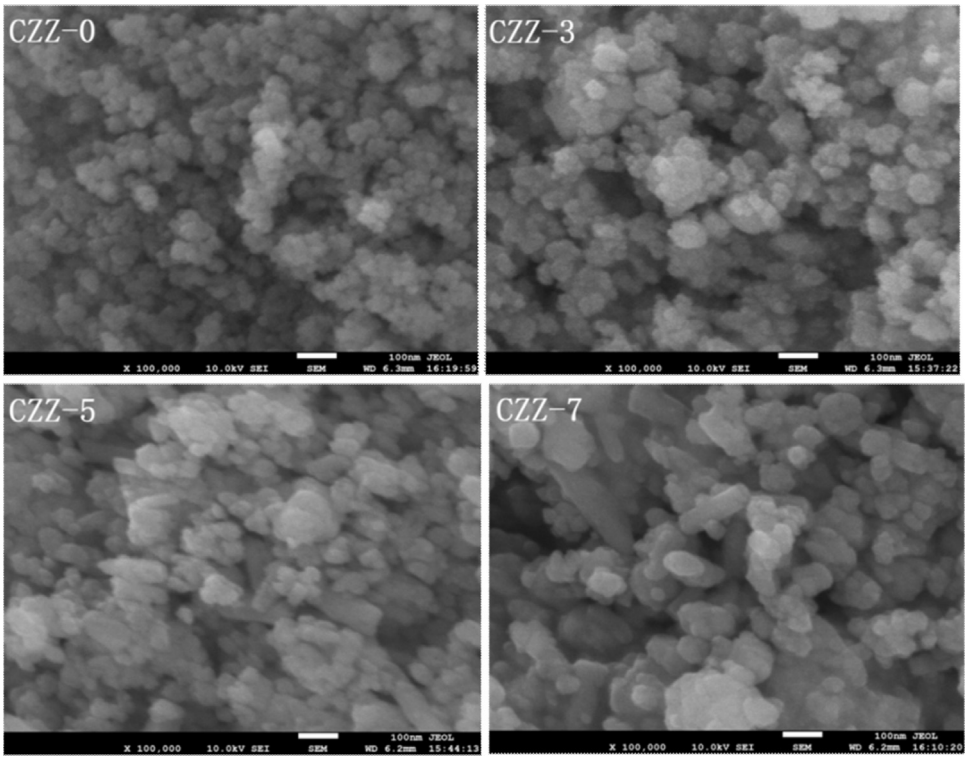

Fig. 4. SEM images of the $Cu/ZnO/ZrO_2$ catalysts.

Table 1
Physicochemical properties of the $Cu/ZnO/ZrO_2$ catalysts.

Sample	BET surface area ($m^2\ g^{-1}$)	Cu surface area($m^2\ g^{-1}$)[a]	d_{Cu}[b] (nm)	Total weight loss (%)	The ratio of different Cu species(%)[c]	
					Cu^+/Cu^{2+}	Cu^0/Cu^+
CZZ-0	77.3	49.0	24.5	22.8	0	12.0
CZZ-3	65.6	31.9	17.5	15.7	1.49	5.14
CZZ-5	56.1	34.4	15.0	10.7	3.03	6.88
CZZ-7	45.3	25.3	14.7	8.9	3.29	3.14

[a] Calculated by N_2O dissociative adsorption.
[b] Calculated by Cu (111) reflection of the XRD results based on Scherrer equation.
[c] Calculated by Cu LMM Auger electron spectroscopy. Cu^+/Cu^{2+} is related to the catalysts after calcination and Cu°/Cu^+ is related to the catalysts after treatment with gas phase.

distribution area of Zn is consistent with the shape of the rodlike particle. The distribution of Zr is similar to that of Cu. Fig. 7(a) and (b) present the HRTEM images of spherical particle and rodlike particle in CZZ-5 sample, respectively. The lattice fringes of spherical particles in Fig. 7(a) are a little disorderly compared with (b) and the measured lattice distance of 0.246 nm corresponds to the spacing of (1 1 1) plane of Cu_2O, implying Cu_2O has a poor crystallinity, which can be seen in the XRD patterns. Fig. 7(b) clearly shows well-defined lattice fringes and the distance between two parallel lattice fringes is measured to be about 0.281 nm, which corresponds to the spacing of (1 0 0) plane of ZnO. It seems that the precipitation-reduction process which deoxidizes Cu species selectively from the co-precipitation slurry leads to a separated phenomenon that the amorphous ZnO particles grow into rodlike particles with good crystallinity while Cu species still exist in the form of spherical particles with a poor crystallinity.

3.2. XPS analysis

Fig. 8 presents the Cu LMM Auger electron spectroscopies of the $Cu/ZnO/ZrO_2$ catalysts. For CZZ-3 ~ 7 samples, a principal peak at around 916.8 eV and a smaller peak at around 917.9 eV are observed, which can be assigned to Cu^+ and Cu^{2+} species, respectively [31,38]. While for CZZ-0 sample, only a peak at around 917.9 eV attributed to Cu^{2+} species can be found. The Cu species in conventional $Cu/ZnO/ZrO_2$ catalysts exists in the form of Cu^{2+} [39] while most Cu^{2+} are reduced to Cu^+ after the reduction with $NaBH_4$. The ratio of Cu^+/Cu^{2+} of the $Cu/ZnO/ZrO_2$ catalysts listed in Table 1 illustrates that the amount of Cu^{2+} reduced to Cu^+ increases with increasing $NaBH_4$ content. The Cu LMM Auger electron spectroscopies of CZZ-0 sample reduced in H_2 at 503 K for 2 h and CZZ-3 ~ 7 samples treated in feed gas (H_2:CO_2 = 3:1) under the same conditions are shown in Fig. 9. After treatment with H_2 or feed gas, the Cu species exist in the form of Cu° (918.65 eV) and Cu^+ (916.8 eV) [31,38], the ratio of which is also listed in Table 1. The value of Cu^0/Cu^+ for CZZ-0 is obvious higher than that of other samples and it increases firstly and then decreases with increasing $NaBH_4$ content for CZZ-3 ~ 7 samples.

3.3. The reducibility of the $Cu/ZnO/ZrO_2$ catalysts

In order to investigate the reduction behavior of the catalysts, TPR measurements were performed. As shown in Fig. 10, the samples exhibit a broad reduction profiles with shoulders in the temperature range of 410–510 K. For further investigation of the TPR results, all profiles are deconvoluted into several Gaussian

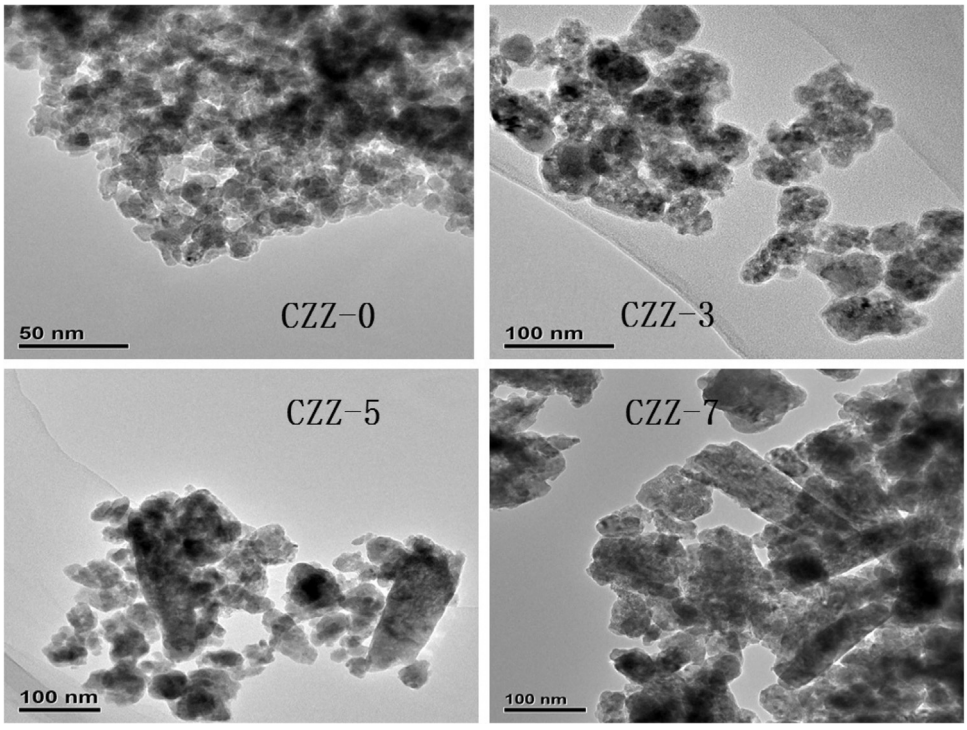

Fig. 5. TEM images of the $Cu/ZnO/ZrO_2$ catalysts.

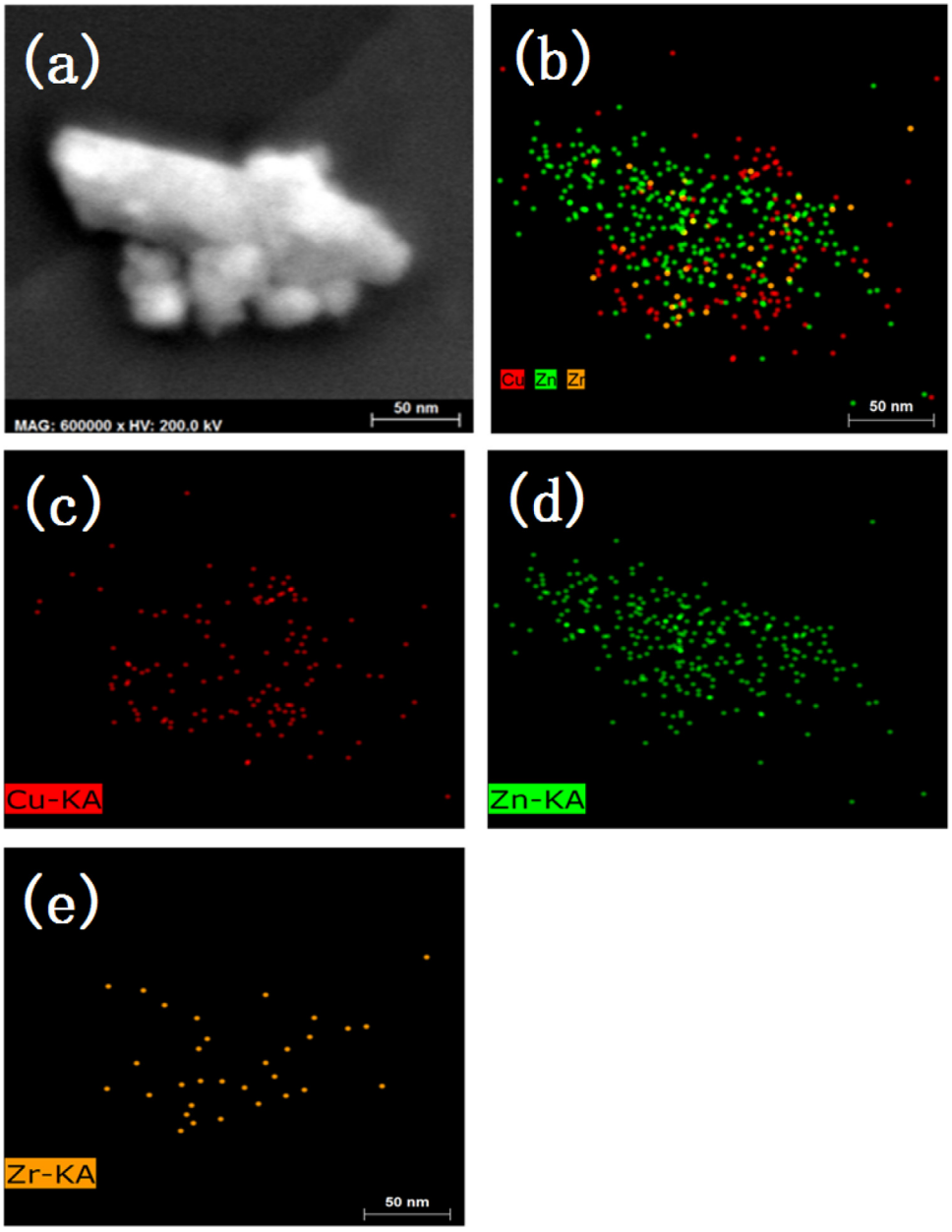

Fig. 6. Elemental map of CZZ-5 sample obtained by STEM-EDS. (a) STEM image of CZZ-5; (b) STEM-EDS elemental map; (c) Cu channel; (d) Zn channel; (e) Zr channel.

Table 2
Temperature of the reduction peaks and their contributions to the TPR pattern of the $Cu/ZnO/ZrO_2$ catalysts.

Sample	TPR peak position [temperature (K)] and concentration(%)[a]		
	Peak α	Peak β	Peak γ
CZZ-0	–	–	469 (100)
CZZ-3	427 (21.6)	454 (44)	476 (34.4)
CZZ-5	437(45.5)	456 (54.5)	–
CZZ-7	430 (40.4)	449 (59.6)	–

[a] Values in parentheses are the contribution (%) of each species.

peaks. The peak position and relative concentration are summarized in Table 2.

The peaks α, β and γ can be ascribed to different aggregation state (dispersed or bulk phase) of CuO, Cu_2O or their combination, which represent Cu species with different reduction capacity. For CZZ-0 prepared by conventional co-precipitation method, only the high temperature peak (peak γ) appears which can be attributed to the reduction of CuO. Reduction peaks appearing in CZZ-3 ~ 7 samples demonstrates that there still exist reducible Cu species (Cu^{2+} and Cu^{+} species) after being reduced by $NaBH_4$, which are in accordance with the results of XRD and XPS. As shown in Fig. 10 and Table 2, the reduction peak α and peak β at lower temperature are observed upon the addition of $NaBH_4$, suggesting that the introduction of $NaBH_4$ leads to an easier reduction of the catalysts. Furthermore, with increasing $NaBH_4$ amount, the reduction peaks shift to lower temperature and no peak γ at high temperature is observed for CZZ-5 and CZZ-7. The difference between CZZ-0 and CZZ-3 ~ 7 indicates that new Cu species whose interaction with other metal oxides is changed by the precipitation-reduction process are produced, thus improving the reducibility of Cu species. A maximum fraction (45.5%) of the peak α to the TPR pattern is found in CZZ-5.

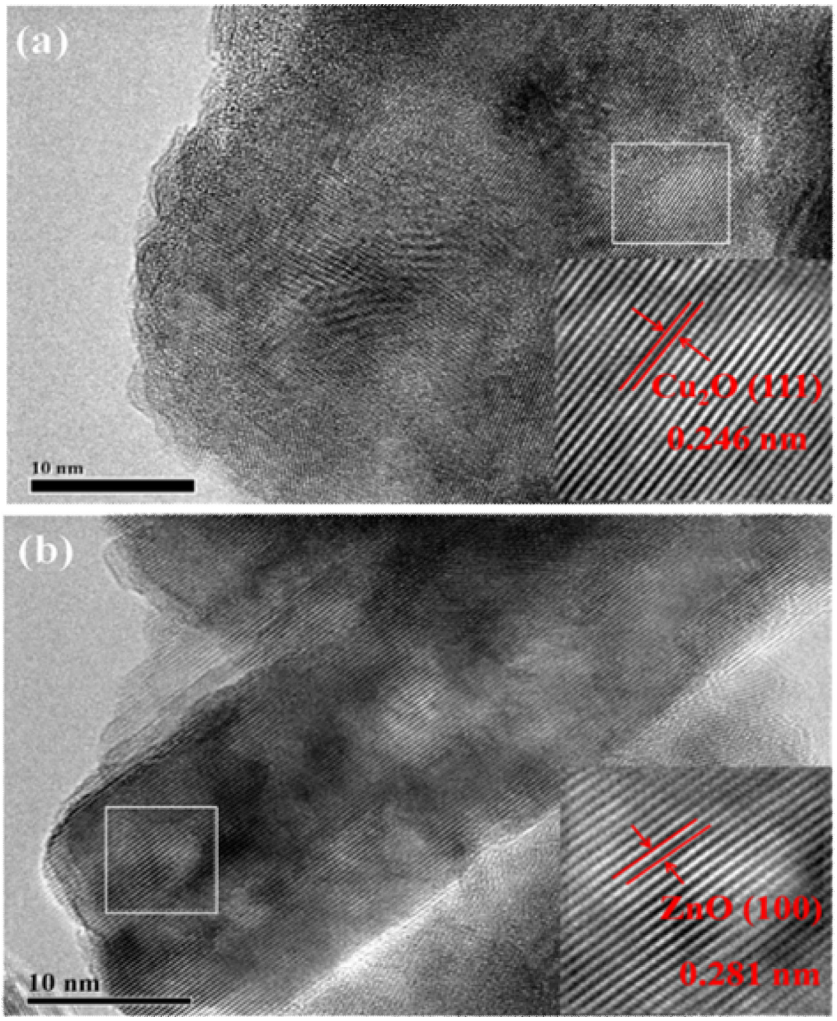

Fig. 7. HRTEM images of spherical particle (a) and rodlike particle (b) in CZZ-5 sample.

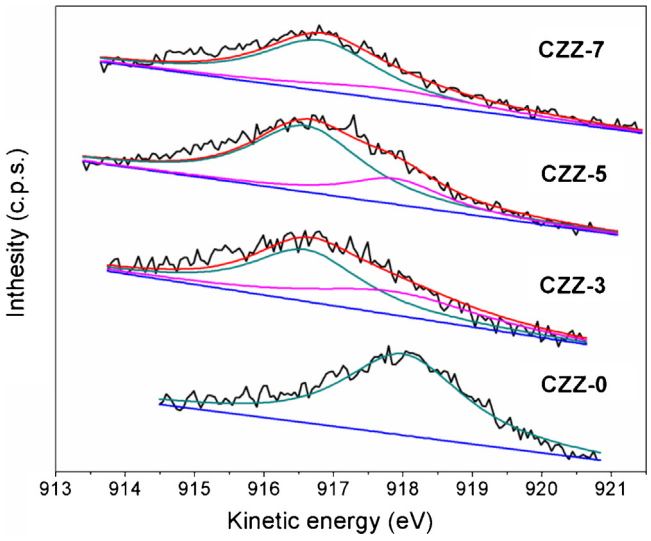

Fig. 8. Cu LMM Auger electron spectroscopies of the $Cu/ZnO/ZrO_2$ catalysts.

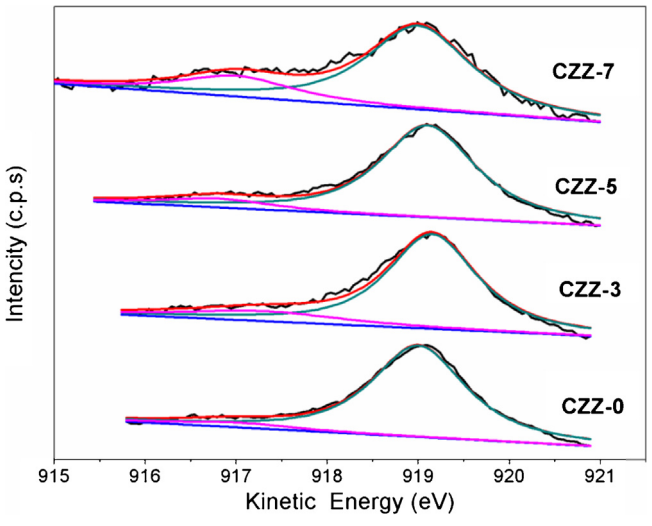

Fig. 9. Cu LMM Auger electron spectroscopies of the $Cu/ZnO/ZrO_2$ catalysts after treatment with gas phase.

3.4. The surface basicity of the $Cu/ZnO/ZrO_2$ catalysts

Fig. 11 shows the CO_2 desorption profiles after pretreatment at 503 K by feed gas over $Cu/ZnO/ZrO_2$ catalysts. The CO_2 desorption profiles at above 573 K (the calcination temperature) were not presented for eliminating the interference of CO_2 produced by thermal decomposition. The profiles can be assigned to two peaks, which represent two types of basic sites. The weakly basic sites (denoted

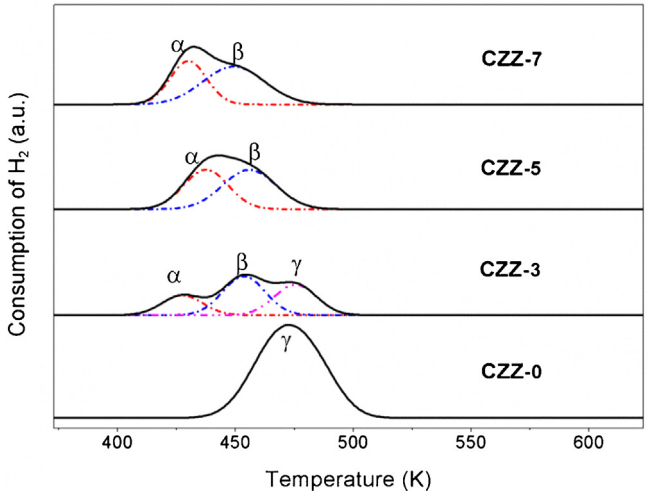

Fig. 10. TPR patterns of the Cu/ZnO/ZrO_2 catalysts.

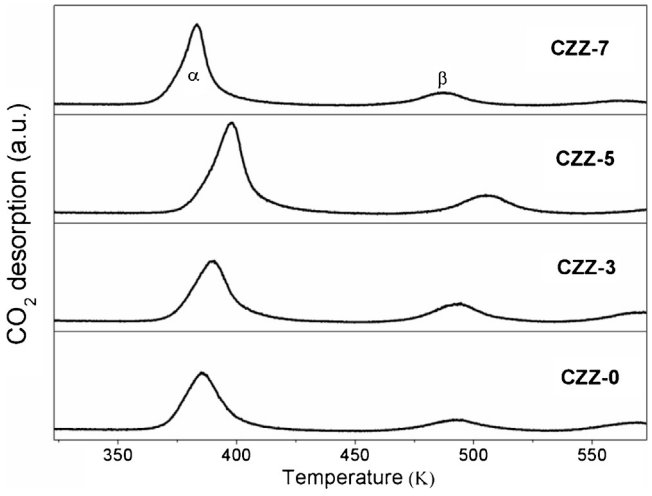

Fig. 11. CO_2-TPD patterns of the Cu/ZnO/ZrO_2 catalysts.

as peak α) can be related to OH^- group, and the moderately basic sites (denoted as peak β) can be assigned to metal-oxygen pairs (such as Zn-O, Zr-O) [5,40]. The number of basic sites in this paper is referred to weakly and moderately basic sites, whose desorption temperature are below 573 K. The quantitative data of basic sites and peak positions listed in Table 3 reveal that the catalysts reduced by $NaBH_4$ possess more basic sites than the CZZ-0 sample. The precipitation-reduction process improves the surface basicity of the catalysts and the amount of basic sites as well as their strength of basic sites first increase until B/Cu = 5 and then decrease. It is known that zirconia possesses surface Lewis basic sites to adsorb CO_2 and it is expected that the alkaline ZnO enhances the affinity of the system to CO_2 [6,9]. The interaction between each component is changed by the precipitation-reduction process, which affects the

Table 3
The amount and distribution of basic sites of the Cu/ZnO/ZrO_2 catalysts.

Sample	Number of basic sites (μmol/g)	CO_2-TPD peak position [temperature (K)]	
		Peak α	Peak β
CZZ-0	40.0	384	485
CZZ-3	50.2	389	492
CZZ-5	59.4	398	502
CZZ-7	44.1	383	484

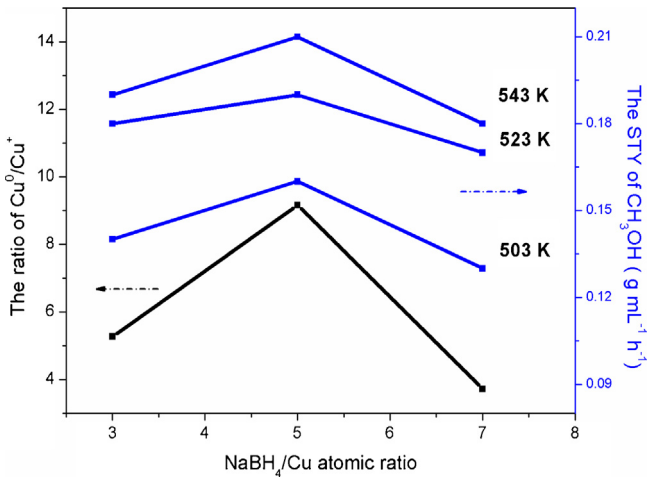

Fig. 12. Effect of $NaBH_4$ content on the ratio of Cu^0/Cu^+ and the STY of CH_3OH over Cu/ZnO/ZrO_2 catalysts.

electronic effect, and thus a great influence on the surface basicity is generated.

3.5. Catalytic performance over Cu/ZnO/ZrO_2 catalysts

The catalytic activities of the Cu/ZnO/ZrO_2 catalysts reduced by different $NaBH_4$ content are listed in Table 4. In particular, CO_2 hydrogenation can be described by a reaction network involving (1) the synthesis of methanol and (2) the reverse water-gas shift (RWGS). The two competitive reactions can be described as follows:

$$CO_2 + 3H_2 \rightarrow CH_3OH + H_2O \quad \Delta H = -49.5 kJmol^{-1} \tag{1}$$

$$CO_2 + H_2 \rightarrow CO + H_2O \quad \Delta H = +41.2 kJmol^{-1} \tag{2}$$

Methanol and CO are the only carbon-containing products under the reaction conditions. As the catalytic activities shown in Table 4, CO_2 conversion increases while CH_3OH decreases with increasing reaction temperature from 503 K to 543 K, a fact that is consistent with other reports [11,12,41]. Actually, increasing temperature facilitates the activation and conversion of CO_2, nevertheless, the production of CO is more favorable than that of methanol due to the endothermic character and higher apparent activation energy of RWGS reaction [41], which are in agreement with the above experimental results. The CO_2 equilibrium conversions calculated at the reaction conditions from the Reactions (1) and (2) are also listed in Table 4. It can be seen that CO_2 conversion increases and gradually approaches to equilibrium with increasing reaction temperature, indicating that CO_2 conversion could be improved kinetically with the temperature increasing from 503 K to 543 K. The catalysts prepared by precipitation-reduction method show an obvious advantage in methanol selectivity over the conventional Cu/ZnO/ZrO_2 catalyst, especially at 503 K. The CH_3OH selectivity is 66.8% over CZZ-5 sample at 503 K, which is 12.7% higher than that over CZZ-0 sample. A maximum STY of CH_3OH of 0.21 g ml^{-1} h^{-1} with CO_2 conversion of 23% and CH_3OH selectivity of 56.8% is obtained over CZZ-5 at 543 K.

The relationship between the STY of CH_3OH, the ratio of Cu^0/Cu^+ and $NaBH_4$ content is shown in Fig. 12. The ratio of Cu^0/Cu^+ first increases and then decreases with B/Cu atomic ratio from 3 to 7, and the STY of CH_3OH presents a similar trend at 503 ~ 543 K. The STY of CH_3OH is related to the ratio of Cu^0/Cu^+, demonstrating that both Cu^+ and Cu^0 species are believed to contribute to the activity and a suitable ratio of Cu^0/Cu^+ is important for the catalytic performance, and similar results have been reported in literature [30,32,33,42]. Therefore, the ratio of Cu^0/Cu^+ on the surface of Cu/ZnO/ZrO_2

Table 4
Catalytic performance for CO_2 hydrogenation to methanol over $Cu/ZnO/ZrO_2$ catalysts.

Temperature (K)	CO_2 equilibrium conversion (%)	Sample	CO_2 conversion (%)	Selectivity (C-mol%)		STY of CH_3OH ($g\,mL^{-1}\,h^{-1}$)
				CH_3OH	CO	
503	28.5	CZZ-0	16.7	54.7	45.3	0.14
		CZZ-3	15.0	62.3	37.7	0.14
		CZZ-5	15.4	66.8	33.2	0.16
		CZZ-7	14.4	60.9	39.1	0.13
523	25.8	CZZ-0	20.3	53.3	46.7	0.17
		CZZ-3	20.0	57.4	42.6	0.18
		CZZ-5	21.0	59.4	40.6	0.19
		CZZ-7	19.4	56.5	43.5	0.17
543	24.6	CZZ-0	22.5	51.8	48.2	0.18
		CZZ-3	21.9	54.4	45.6	0.19
		CZZ-5	23.0	56.8	43.2	0.21
		CZZ-7	21.7	53.3	46.7	0.18

Reaction conditions: P = 5.0 MPa, n(H2):n(CO2) = 3:1, GHSV = 4600 h-1.

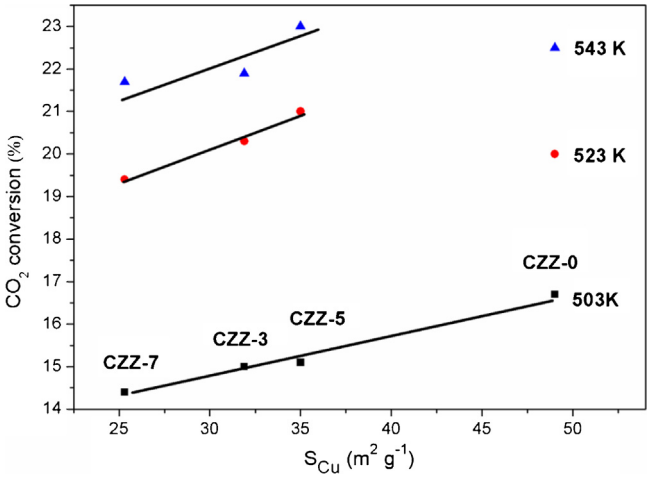

Fig. 13. The relationship between the CO_2 conversion and the Cu surface area over $Cu/ZnO/ZrO_2$ catalysts.

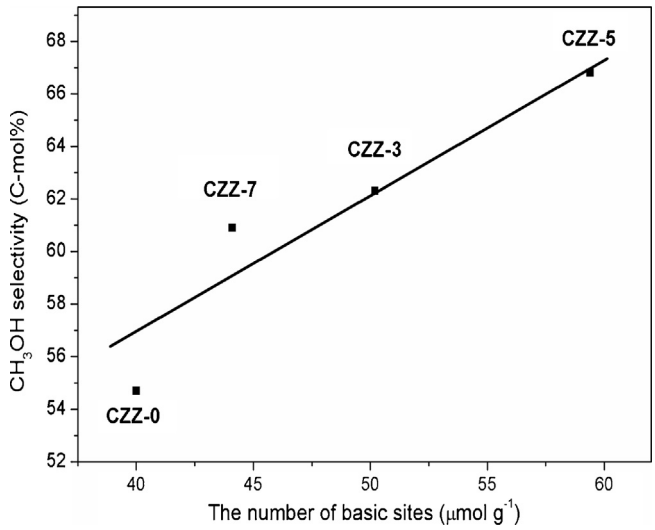

Fig. 14. The relationship between CH_3OH selectivity and the number of basic sites over $Cu/ZnO/ZrO_2$ catalysts.

catalysts obtained from precipitation-reduction method could be optimized to a certain extent via controlling $NaBH_4$ content and thus improving the activity of the catalysts.

According to the mechanism of CO_2 hydrogenation to methanol, the exposed copper surface area (S_{Cu}) is an important parameter and the relationship between S_{Cu} and catalytic performance has been studied comprehensively [10,11,14,27,28,30,41,43]. In this study, CO_2 conversion increases with the increase of the exposed copper surface area at 503 K which is shown in Fig. 13, and a near linear relationship exists between them. The results can be explained as follows: a large value of S_{Cu} leads to more dissociatively adsorbed H_2 and then provides a source of atomic hydrogen by spillover to ZnO or ZrO_2. Furthermore, it is noteworthy that CO_2 conversion and S_{Cu} do not live up to the near linear relationship any more at 523 K and 543 K. CZZ-0 sample shows a relative poor CO_2 conversion while the catalysts reduced by $NaBH_4$ still accord with the above rule. The possible reasons are interpreted as follows: compared with the catalysts obtained by conventional co-precipitation method, the Cu species in catalysts prepared by precipitation-reduction method have stronger ability against agglomeration when undergoing heat treatment, and these advantages become manifest with the elevation of reaction temperature. The XRD results also illustrate that the growth of Cu grain crystals during treatment with gas phase in CZZ-3 ~ 7 samples is slower.

As illustrated above, the CH_3OH selectivity over the $Cu/ZnO/ZrO_2$ catalysts first increases and then decreases with increasing $NaBH_4$ content. Although some factors affecting the methanol selectivity have been proposed, the conclusions are far from agreement up to now. Rhodes and Bell investigated the effect of zirconia phase on the activity and selectivity over Cu/ZrO_2 catalysts and found that the selectivity over Cu/m-ZrO_2 was remarkably higher than that over Cu/t-ZrO_2 [44,45]. Gao et al. prepared a series of Cu/Zn/Al/Zr catalysts via hydrotalcite-like precursors with different Zr content and claimed that the CH_3OH selectivity was related to the distribution of basic sites on the surface [5]. Furthermore, the La-M-Cu-Zn-O catalysts derived from perovskite-type precursors showed high selectivity for methanol and the high CH_3OH selectivity was confirmed to correlate with the Cuα species [14]. In this study, the CH_3OH selectivity increases with the increase of the amount of basic sites. To better disclose their relationship, a plot of CH_3OH selectivity versus the amount of basic sites is presented. As shown in Fig. 14, an approximately linear relationship exists between CH_3OH selectivity and the amount of basic sites.

Many studies have demonstrated that mixed surface sites on Cu, ZnO and ZrO_2 contribute to the activation of H_2, CO and CO_2 over $Cu/ZnO/ZrO_2$ catalysts. Guo et al. proposed that the Cu sites served to dissociatively adsorb H_2 and to provide a source of atomic hydrogen by spillover, and ZnO and ZrO_2 tended to adsorb CO_2 as bicarbonate species which undergone stepwise hydrogenation to form methanol [43]. Furthermore, many reports proposed there was a synergetic effect between Cu and the promoter, which

was considered to contribute to the catalytic performance [46,47]. Therefore, the bifunctional mechanism is currently accepted.

Based on above discussions, the mechanism of the Cu/ZnO/ZrO_2 catalysts prepared by precipitation-reduction method for CO_2 hydrogenation to methanol accords with the bifunctional mechanism.

4. Conclusions

A series of Cu/ZnO/ZrO_2 catalysts reduced by different $NaBH_4$ content were prepared by precipitation-reduction method for CO_2 hydrogenation to methanol. The content of $NaBH_4$ has a significant influence on the physicochemical properties and catalytic performance. Based on the above results, the following conclusions can be drawn:

(1) Compared with conventional co-precipitation method, catalysts with smaller Cu particles are much more easily to be obtained by means of precipitation-reduction method.
(2) For the catalysts obtained from precipitation-reduction method, the viewpoint that both Cu^+ and Cu^0 species are contributed to the activity of CO_2 hydrogenation to methanol is accepted. The STY of CH_3OH is related to the ratio of Cu^0/Cu^+ which can be optimized to a certain extent by varying the $NaBH_4$ content and thus improving the activity of the catalysts.
(3) The mechanism of the Cu/ZnO/ZrO_2 catalysts prepared by precipitation-reduction method for CO_2 hydrogenation to methanol accords with the bifunctional mechanism. The CO_2 conversion is related to the exposed Cu surface area and the CH_3OH selectivity is connected with the amount of basic sites.
(4) A maximum CH_3OH selectivity of 66.8% is obtained with B/Cu = 5at 503 K.

Acknowledgements

This work was financially supported by the Key Science and Technology Program of Shanxi Province, China (MD2014-10), the National Key Technology Research and Development Program of the Ministry of Science and Technology (2013BAC11B00), and the Natural Science Foundation of China (21343012).

References

[1] G.A. Olah, A. Goeppert, G.K.S. Prakash, J. Org. Chem. 74 (2009) 487–498.
[2] G.A. Olah, G.K.S. Prakash, A. Goeppert, J. Am. Chem. Soc. 133 (2011) 12881–12898.
[3] M. Behrens, J. Catal. 267 (2009) 24–29.
[4] O. Martin, J. Perez-Ramirez, Catal. Sci. Technol. 3 (2013) 3343–3352.
[5] P. Gao, F. Li, H. Zhan, N. Zhao, F. Xiao, W. Wei, L. Zhong, H. Wang, Y. Sun, J. Catal. 298 (2013) 51–60.
[6] F. Arena, G. Italiano, K. Barbera, S. Bordiga, G. Bonura, L. Spadaro, F. Frusteri, Appl. Catal. A 350 (2008) 16–23.
[7] J. Sloczynski, R. Grabowski, P. Olszewski, A. Kozlowska, J. Stoch, M. Lachowska, J. Skrzypek, Appl. Catal. A 310 (2006) 127–137.
[8] G. Bonura, M. Cordaro, C. Cannilla, F. Arena, F. Frusteri, Appl. Catal. B 152–153 (2014) 152–161.
[9] F. Arena, G. Italiano, K. Barbera, G. Bonura, L. Spadaro, F. Frusteri, Catal. Today 143 (2009) 80–85.
[10] P. Gao, F. Li, N. Zhao, F. Xiao, W. Wei, L. Zhong, Y. Sun, Appl. Catal. A 468 (2013) 442–452.
[11] F. Arena, G. Mezzatesta, G. Zafarana, G. Trunfio, F. Frusteri, L. Spadaro, J. Catal. 300 (2013) 141–151.
[12] F. Arena, K. Barbera, G. Italiano, G. Bonura, L. Spadaro, F. Frusteri, J. Catal. 249 (2007) 185–194.
[13] C. Jeong, Y.-W. Suh, Catal. Today 265 (2016) 254–263 http://dx.doi.org/10.1016/j.cattod.2015.07.053.
[14] H. Zhan, F. Li, P. Gao, N. Zhao, F. Xiao, W. Wei, L. Zhong, Y. Sun, J. Power Sources 251 (2014) 113–121.
[15] K. Schutte, H. Meyer, C. Gemel, J. Barthel, R.A. Fischer, C. Janiak, Nanoscale 6 (2014) 3116–3126.
[16] A. García-Trenco, A. Martínez, Catal. Today 215 (2013) 152–161.
[17] E. Frei, A. Schaadt, T. Ludwig, H. Hillebrecht, I. Krossing, ChemCatChem 6 (2014) 1721–1730.
[18] S. Fujita, S. Moribe, Y. Kanamori, M. Kakudate, N. Takezawa, Appl. Catal. A 207 (2001) 121–128.
[19] E. Batyrev, J. Vandenheuvel, J. Beckers, W. Jansen, H. Castricum, J. Catal. 229 (2005) 136–143.
[20] X.-M. Liu, G.Q. Lu, Z.-F. Yan, J. Beltramini, Ind. Eng. Chem. Res. 42 (2003) 6518–6530.
[21] L. Shi, W. Shen, G. Yang, X. Fan, Y. Jin, C. Zeng, K. Matsuda, N. Tsubaki, J. Catal. 302 (2013) 83–90.
[22] L. Shi, Y. Tan, N. Tsubaki, ChemCatChem 4 (2012) 863–871.
[23] L. Shi, K. Tao, R. Yang, F. Meng, C. Xing, N. Tsubaki, Appl. Catal. A 401 (2011) 46–55.
[24] S. Belin, C.L. Bracey, V. Briois, P.R. Ellis, G.J. Hutchings, T.I. Hyde, G. Sankar, Catal. Sci. Technol. 3 (2013) 2944–2957.
[25] B.J. Liaw, Y.Z. Chen, Appl. Catal. A 206 (2001) 245–256.
[26] J. Yoshihara, C.T. Campbell, J. Catal. 161 (1996) 776–782.
[27] W.X. Pan, R. Cao, D.L. Roberts, G.L. Griffin, J. Catal. 114 (1988) 440–446.
[28] S. Natesakhawat, J.W. Lekse, J.P. Baltrus, P.R. Ohodnicki, B.H. Howard, X. Deng, C. Matranga, ACS Catal. 2 (2012) 1667–1676.
[29] R.G. Herman, K. Klier, G.W. Simmons, B.P. Finn, J.B. Bluko, J. Catal. 56 (1979) 407–429.
[30] M. Saito, T. Fujitani, M. Takeuchi, T. Watanabe, Appl. Catal. A 138 (1996) 311–318.
[31] P. Gao, F. Li, F. Xiao, N. Zhao, N. Sun, W. Wei, L. Zhong, Y. Sun, Catal. Sci. Technol. 2 (2012) 1447–1454.
[32] J. Toyir, P. Ramírez de la Piscina, J.L.G. Fierro, N. Homs, Appl. Catal. B 34 (2001) 255–266.
[33] J. Toyir, P. Ramírez de la Piscina, J.L.G. Fierro, N. Homs, Appl. Catal. B 29 (2001) 207–215.
[34] G.C. Chinchen, K.C. Waugh, J. Catal. 97 (1986) 280–283.
[35] R. Yang, X. Yu, Y. Zhang, W. Li, N. Tsubaki, Fuel 87 (2008) 443–450.
[36] C. Baltes, S. Vukojevic, F. Schuth, J. Catal. 258 (2008) 334–344.
[37] P. Gao, R. Xie, H. Wang, L. Zhong, L. Xia, Z. Zhang, W. Wei, Y. Sun, J. CO_2 Util. 11 (2015) 41–48.
[38] J. Słoczyński, R. Grabowski, A. Kozłowska, P. Olszewski, J. Stoch, J. Skrzypek, M. Lachowska, Appl. Catal. A 278 (2004) 11–23.
[39] P. Gao, L. Zhong, L. Zhang, H. Wang, N. Zhao, W. Wei, Y. Sun, Catal. Sci. Technol. 5 (2015) 4365–4377.
[40] G. Wu, X. Wang, W. Wei, Y. Sun, Appl. Catal. A 377 (2010) 107–113.
[41] X. Guo, D. Mao, G. Lu, S. Wang, G. Wu, J. Catal. 271 (2010) 178–185.
[42] G. Wang, Y. Zhao, Z. Cai, Y. Pan, X. Zhao, Y. Li, Y. Sun, B. Zhong, Surf. Sci. 465 (2000) 51–58.
[43] X. Guo, D. Mao, G. Lu, S. Wang, G. Wu, J. Mol. Catal. A: Chem. 345 (2011) 60–68.
[44] M. Rhodes, K. Pokrovski, A. Bell, J. Catal. 233 (2005) 210–220.
[45] M. Rhodes, A. Bell, J. Catal. 233 (2005) 198–209.
[46] R. Burch, S.E. Golunki, M.S. Spencer, J. Chem. Soc. Faraday Trans. 86 (1990) 2683–2691.
[47] H.Y. Chen, S.P. Lau, L. Chen, J. Lin, C.H.A. Huan, K.L. Tan, J.S. Pan, Appl. Surf. Sci. 152 (1999) 193–199.